

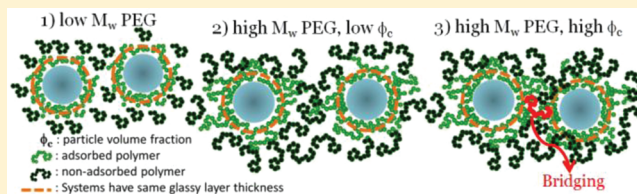
Polymer Dynamics in PEG-Silica Nanocomposites: Effects of Polymer Molecular Weight, Temperature and Solvent Dilution

So Youn Kim,^{†,§} Henriette W. Meyer,[‡] Kay Saalwächter,^{*,‡} and Charles F. Zukoski^{*,†}

[†]Department of Chemical & Biomolecular Engineering, University of Illinois, Urbana, Illinois 61801, United States

[‡]Institut für Physik—NMR, Martin-Luther-Universität Halle-Wittenberg, Betty-Heimann-Strasse 7, D-06120 Halle, Germany

ABSTRACT: The mechanical properties of particulate nanocomposites strongly depend upon the particle dispersion, as well as on the closely related properties in thin polymer films covering the particle surface. The length scale of such changes is relevant for the understanding of particle–particle interactions, which ultimately dominate the mechanical response. Using well-defined 44 nm diameter silica nanoparticles dispersed in poly(ethylene glycol), we focus on surface-induced changes in polymer dynamics. Using proton time-domain NMR, we distinguish three polymer phases of different mobility, i.e., a strongly adsorbed, solid-like fraction, a fraction with intermediate relaxation times and a highly mobile fraction. We explore how these fractions change as we vary polymer molecular weight from 300 to 20 000 and particle volume fraction up to 0.3. A multiple-quantum experiment enables a closer analysis of the mobile component which we show consists of two fractions, one resembling the bulk melt-like and another one showing network-like properties. We demonstrate that above a polymer molecular weight-dependent volume fraction, polymers form elastically active links between particles, resulting in the physical gelation observed in such systems. Our results provide a quantitative picture of network formation, which is described by the amount and length of network-like chains as well as heterogeneities in the polymer dynamics. We relate changes in polymer dynamics to particle microstructure obtained from small angle neutron scattering.



I. INTRODUCTION

Polymer nanocomposites have been spot-lighted due to enhanced mechanical, optical and/or rheological properties created when nanoparticles are introduced into a polymeric matrix.^{1–4} A particular class of such materials is represented by particle-filled polymer melts, which often exhibit strong mechanical reinforcement.^{5–8} The properties of such materials are important in developing a molecular-level understanding of filled, cross-linked elastomers, which are a highly relevant class of every-day nanomaterials. However, the development and optimization of these materials are still mostly based on empirical strategies.^{9,10}

One distinct feature of polymer nanocomposites is that, due to their high inner surface area, strong interactions between nanoparticle surface and polymer chains are thought to be enhanced and ultimately responsible for the large changes of the mechanical properties over those of a bulk polymer melt or elastomer.^{8,11} These effects occur at the molecular level and are associated with changes in polymer dynamics created by polymer adsorption to the particle surfaces.^{12–16} Not all polymer particle mixtures show these enhancements, raising questions about the length scale over which polymer dynamics are influenced and how alterations in polymer dynamics are dependent on the specific chemistry of polymer-surface system under investigation.

Changes in polymer dynamics due to the presence of closely spaced solid surfaces can be inferred from changes in composite glass transition temperature (T_g),^{17,18} yet care has to be taken

when such changes are deduced from the bulk mechanical properties, as recently highlighted by Robertson et al.¹⁹ Characterizing how surfaces alter polymer dynamics calls for molecular-level techniques, such as inelastic neutron scattering,^{20,21} dielectric spectroscopy,¹⁴ or NMR spectroscopy. The latter, in particular when performed on protons in the time domain, using low-field equipment, can yield detailed insights into as-made materials.^{12,13,16,22–26}

In particular for the system of fumed or precipitated silica-poly(dimethylsiloxane), multiple hydrogen bonds between surface-OH groups and the locally polar PDMS main chains were shown to lead to a 1–2 nm layer of strongly immobilized (often referred to as “glassy”) polymer layer irrespective of the end-groups or whether the chains are grafted or adsorbed to the particle surfaces.^{13–15} The strength of the adsorption layer and thus the overall reinforcement effect in composites was shown to decrease with an increase of surface water content,^{27,28} and surface modification of the silica by silanization, rendering it more hydrophobic, was demonstrated to decrease its affinity toward PDMS and other fluids capable of forming hydrogen bonds.^{22,29,30} Our recent work demonstrates that a fraction of chains forming elastically active bridges between the particles is responsible for the formation of physical gels even with linear PDMS of high molecular weight (but without cross-links), and

Received: March 5, 2012

Revised: April 17, 2012

Published: May 4, 2012

we also found a corresponding negative effect of hydrophobic silanization agents.²⁶

Extensive studies of the silica–poly(ethyl acrylate) system demonstrate that polymer segments are also held in a highly confined, glass-like state near the particle surfaces, irrespective of whether the bulk polymer is highly cross-linked or not. Observations were made via the measurement of the free induction decay (FID) NMR time-domain signal for cross-linked poly(ethyl acrylate) filled with well-defined and well-dispersed silica,^{12,16} where the thickness of the immobilized layer was found to vary between 2 and 10 nm, depending on temperature and whether the polymer was just physically adsorbed or covalently grafted to the surface by a specific silanization agent, the latter leading to thicker layers. Additional network effects, i.e., a local increase of the cross-link density close to the particle surface, were in this case only found for the case of chains that are covalently linked to the silica.¹⁶

Corresponding studies on filled poly(ethylene oxide), PEO, or poly(ethylene glycol), PEG (without or with –OH end groups, respectively), are rare. Recently, Krutyeva et al.²⁰ reported the observation of a small immobilized contribution to the inelastic neutron scattering signal, resulting from a glassy/adsorbed layer of PEO in channels of 15 nm diameter in alumina (providing hydrophilic surface similar to silica), but no further “confinement effect” on the majority component on the pico- to nanosecond time scale of their experiment was reported. Complementary to this, neutron spin-echo spectroscopy on the same samples did reveal confinement-induced changes in the chain dynamics (Rouse modes) at a longer time scale on the order of 100 ns. This observation could well be related to our previous observation of an additional network-like component in linear PDMS filled with silica.²⁶

Here we explore these effects in more detail, focusing on the effects of degree of polymerization from below to above entanglement molecular weight (M_e), and where the particle surfaces are brought into close proximity by increasing the particle volume fraction (ϕ_c). Both effects could be expected to enhance the network-like polymer formation. The case of PEG-silica is also advantageous in that the polymer-surface interaction has been characterized in detail and is known to be strongly adsorbing^{31–34} for which there is a broadly accepted consensus that the glass transition temperature locally increases.³⁵ We thus circumvent the controversial issue of T_g effects of different sign for weakly adsorbing polymers, where there is evidence that nonwetting surfaces may enhance polymer relaxation rates and thus decrease T_g .^{36,37} One key limitation in understanding these phenomena lies in developing independent measures of the strength of cohesion of polymer segments to particle surfaces.

In this paper we use proton low-field NMR methods to investigate the effects of dispersing 44 nm silica particles in concentrated PEG solutions and melts. Our goal is to examine the impact of particle volume fraction and solvent dilution on the existence of glassy layers and topologically constrained (network-like) components, in analogy to previous work on the silica–PDMS system.²⁶ We undertake these studies for polymers with molecular weights spanning nearly 2 orders of magnitude (300–20 000 g/mol). This experimental system is chosen because (i) particles are miscible with concentrated polymer solutions and melts, (ii) we can explore the influence of particles on topological constraints in the absence of bulk chemical cross-links, and (iii) these systems have been extensively studied using small angle scattering techniques

and the polymer reference interaction site model (PRISM) to extract the adhesive strength of polymer segment-particle surfaces interactions.^{31,32,34,38} Of particular interest are the effects of increasing volume fraction on the network formation and its relation to the flow properties of the composite. As an example, in Figure 1, we compare two samples composed of

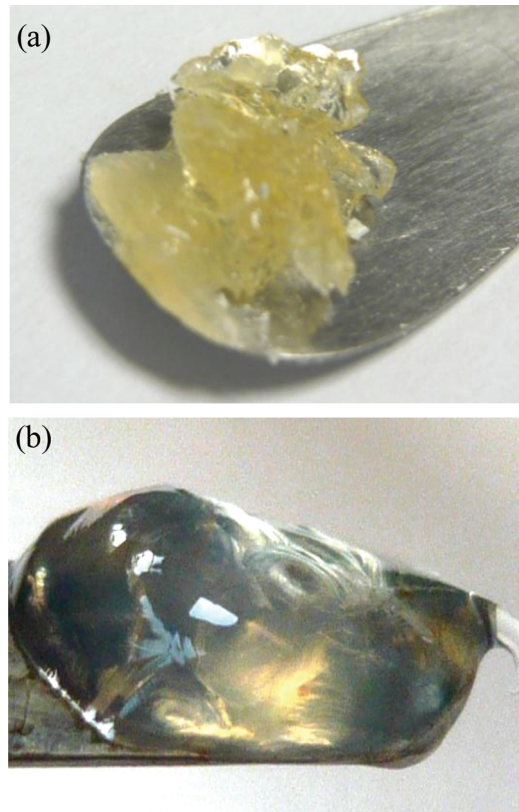


Figure 1. (a) Silica nanoparticles in PEG 8000 at $\phi_c = 0.315$ at $R_p = 1$. (b) Same particles in PEG 8000 at $\phi_c = 0.300$ at $R_p = 0.5$ where R_p is the ratio of polymer volume over the volume of polymer plus solvent.

PEG of 8000 g/mol containing 44 nm silica, both at a particle volume fraction of ~0.30. In Figure 1a the particles are dispersed in the melt, and in the second sample (Figure 1b) the particles are dispersed in a solution that contains 50% by volume polymer and 50% water. The melt sample shows brittle failure, while the diluted sample is a viscous liquid. Below we explore the origin of these differences by investigating polymer mobility at the particle surface and in the bulk, focusing in particular on the formation of network-like components upon changing the particle volume fraction, the polymer molecular weight, and the degree of dilution.

Below we detail how polymer dynamics can be quantified with proton low-field NMR techniques and how polymer segment relaxation processes are altered in the presence of particles as functions of filler concentration, temperature, polymer molecular weight and dilution with solvent, providing a molecular-level explanation of the behavior highlighted in Figure 1. Exploiting magic-sandwich echo (MSE) experiments, which refocus the initial part of the free-induction decay (FID) and thus avoid the dead-time issue, we were able to quantitatively capture the solid-like signal components that relax on short time scales of less than 30 μ s.³⁹ On the other hand, multiple-quantum (MQ) experiments²⁵ were carried out

to investigate the presence of topological constraints such as surface links (possibly in combination with trapped entanglements), which lead to relaxation phenomena on a slower time scale of 0.1–10 ms. While previous work on PDMS-silica was restricted to qualitative decompositions of transverse relaxation decays,^{22,23} the MQ experiments provide a sensitive and quantitative measure of the origins of the differences in spin relaxation since they measure the residual dipolar coupling, related to the topologically induced anisotropy of chain motion, directly and on an absolute scale, as demonstrated previously for the case of PDMS-silica.²⁶ Using neutron scattering results to composite microstructure, we further connect the obtained information on the polymer dynamics to the thermodynamic state of particle dispersions, providing a concise picture of the influence of particle surfaces on the segmental and larger-scale dynamics of PEG as exposed to silica surfaces.

II. EXPERIMENTAL SECTION

Sample Preparation. Silica nanoparticles were synthesized based on the method of Stöber et al.,⁴⁰ using the base-catalyzed hydrolysis and condensation of tetraethylorthosilicate (TEOS) yielding particles with diameters of 44 ± 5 nm as determined from both SEM micrographs and fitting the particle form factor determined by the angle dependence of neutron scattering from a dilute suspension. All PEG of varying M_w (included as number in the sample name, in units of g/mol) were purchased from Sigma-Aldrich, and pure ethanol was supplied from Decon Lab. Inc. After particle synthesis, the mixture of particle and ethanol was concentrated approximately 10 times by heating in a ventilation hood. During this process, the excess ammonium hydroxide was removed.

Particle volume fractions (ϕ_c) were calculated using the masses of each component and their densities. The density of the silica particles is 1.6 g/cm³.⁴¹ In making the nanocomposite melts, a defined mass of the mixture of particle and ethanol is mixed with a defined mass of PEG. Samples were heated in a vacuum oven to remove residual ethanol. The vacuum oven was then purged several times with nitrogen followed by evacuation of the chamber to remove oxygen, yielding the investigated polymer nanocomposites. For the preparation of water-diluted particle suspensions, the mass of each component (silica, PEG, D₂O) was determined in order to create the desired particle and polymer concentrations. Once the ethanol was evaporated, the necessary amount of D₂O (to avoid excess water signal and restrict the NMR analyses to the polymer component) was added to the sample to produce the desired concentrations of particles and PEG. Our goal is to produce particles that experience only excluded-volume interactions in the absence of the polymer; in the absence of polymer-induced interactions, the intrinsic particle interactions are those of hard spheres. This is accomplished by working with particles that are index matched to the polymer. In this process, the strength of van der Waals attractions between the particles which depend primarily on polarization interactions at visible frequencies are minimized.⁴²

In all samples the polymer concentration is defined as R_p which is the ratio of polymer volume over the volume of polymer plus solvent. In the absence of solvent, R_p is 1, while $R_p = 0.5$ when polymer solution contains 50% solvent and 50% polymer.

Low-Field NMR. The NMR measurements were performed on a Bruker Minispec mq20 at 20 MHz proton resonance frequency. The sample temperature was controlled with a BVT3000 heater operating on an air flow at temperatures of 70 ± 0.5 and 100 ± 0.5 °C, allowing for sufficient time (ca. 1 h) to stabilize the instrument at each temperature. Samples were loaded in conventional 10 mm diameter NMR tubes and flame-sealed to avoid evaporation. The minispec has typical $\pi/2$ pulse lengths of down to 2 μ s with a reliable phase cycling in $\pi/2$ steps. The number of scans was varied from 128 to 512 depending on the sample conditions to obtain good signals quality, and the recycle delay was varied between 1 and 4 s to ensure complete

relaxation of all components and thus quantitative signal decompositions.

Magic-Sandwich Echo. The shape of the proton NMR time-domain signal is mainly influenced by the ¹H–¹H dipole–dipole couplings, which depend on the average distance between spins and the orientation of the internuclear vectors with respect to the magnetic field. While the protons are fixed in the monomer unit at well-defined distances leading to well-defined strong dipolar couplings (thus reflecting structural information), the orientation effect introduces sensitivity to rotational dynamics. The high mobility in a mobile melt or solution phase results in a strong motional averaging of the dipolar couplings, thus leading narrow spectral lines, and correspondingly in the time domain to rather long transverse relaxation time (τ_m , often referred to as an apparent T_2^*) on the order of milliseconds to seconds. To the contrary, the strong dipolar couplings in a rigid/glassy phase lead to broad spectral lines, corresponding to a fast transverse relaxation of the signal on the time scale of less than 50 μ s (τ_g). The simple measurement of the free-induction decay (FID) NMR time-domain signal thus allows for a quantification of the proton fractions in mobile and rigid environments, based on their qualitatively different relaxation behavior. As detailed below, the challenge at hand is to distinguish a certain number of components of different mobility on the basis of a reliable fit in a system that actually exhibits a range of mobilities that may be described by a gradient in front of a surface.

Although ¹H FID analysis has become popular since it is readily available with low-field NMR spectrometers, the impossibility to detect the first 10–15 μ s of the FID on most spectrometers due to the comparably long ring-down of the strong rf pulse challenges the quantitative fit of the initial rapid decay associated with protons in rigid environments. To avoid this “dead-time” issue, we use the full dipolar time-reversed mixed magic-sandwich echo (MSE), as detailed in ref 39. The MSE (of total minimum duration τ_{MSE} of 6×0.013 ms) refocuses the rapid dipolar dephasing of the signal to form an almost quantitative echo, so detection can start on the echo top and is thus essentially dead-time free (with given τ_{MSE} , the time after the last rf pulse is $\tau_{\text{MSE}}/6$, long enough to overcome the dead time). Figure 2a shows an example of typical FID from a PEG 20000 sample with $\phi_c = 0.4$ at 70 °C, demonstrating the near-quantitative restoration of the initial part of the FID by help of the MSE with a relative intensity loss on the 10% scale. However, noting that the small observed loss can become stronger when some local mobility is present in the glassy layer,¹⁶ we aim at a quantitative correction of the small observed signal loss, using the MSE mainly to get to know the *shape* of the initial signal, enabling a fit to the more quantitative direct FID signal using predetermined shape functions, thus reducing the number of fit parameters in the component decomposition.

To this end, we use magnetization filters to emphasize different signal components. For example, a dipolar “magic and polarization echo” (MAPE) filter,^{39,43} which in essence is a long (thus for rigid components due to a higher-order effect inefficient) MSE applied before the first 90° pulse, is used to remove unwanted contributions from the rigid parts and thus to select the mobile phase. When the duration of the MAPE filter (τ_{MAPE}) is increased to 1.23 ms, the example given in Figure 2a demonstrates that the fast decay from the rigid part no longer contributes, such that the FID signal only contains contributions from the slowly decaying or mobile polymer segments. We note that there is additional loss of intensity when the filter length is further increased, however the shape of the filtered signal stays roughly the same. For all samples studied here we found that $\tau_{\text{MAPE}} = 1.23$ ms was sufficient to remove all fast-relaxing contributions at minimum loss of mobile signal. As shown below, this signal function is used to predetermine the shape parameters of the associated relaxation function for the final fits.

On the other hand, selective magnetization of the rigid phase is realized with a ¹H double-quantum (DQ) filter based on a two-pulse segment that allows for very short DQ excitation times adapted to strong dipolar couplings. Detailed information is again given in ref 39. The selective polarization of the rigid phase by a DQ-filter is based on the excitation of double-quantum coherences in the rigid region, which becomes possible because of the strong dipolar couplings. The

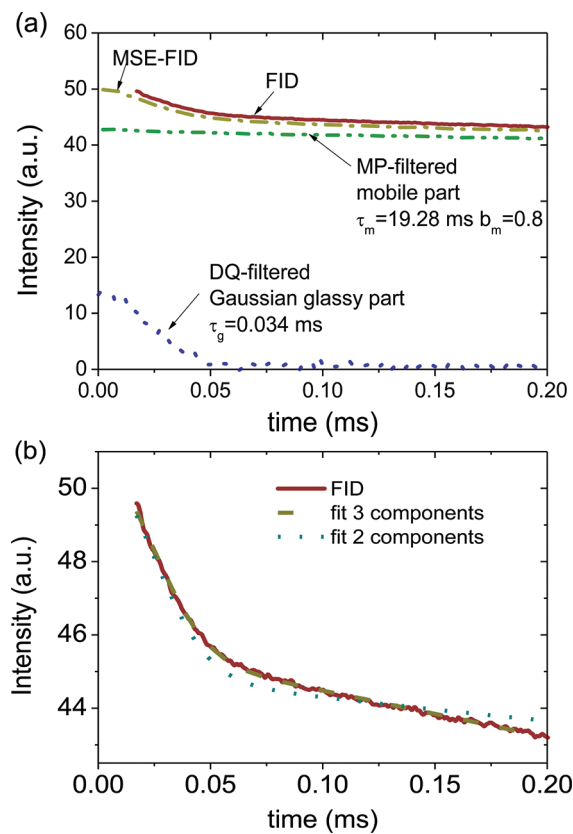


Figure 2. (a) FID, MSE-FID, and MAPE- and DQ-filtered signals as a function of the acquisition time for PEG 20000 at $\phi_c = 0.4$ and 70°C . The DQ-filtered signal is not to scale and is amplified by a factor of 10 for better visibility. (b) Fits to the FID with a sum of 2 or 3 modified exponentials.

efficiency of creating (and filtering for) such DQ coherences depends on the DQ excitation time (τ_{DQ}), which is optimized for maximum intensity in separate experiments. A typical intensity build-up function is given in Figure 3 of ref 39, and similar results were obtained herein. The lowermost curve in Figure 2a shows the DQ-filtered signal based on a $\tau_{\text{DQ}} = 0.030 \text{ ms}$ corresponding to maximum DQ efficiency, which rather evidently reflects only the rigid regions. Note that DQ excitation has an efficiency of less than 50% (typically around 30%), meaning that this signal is not quantitative and thus not to scale. However, the

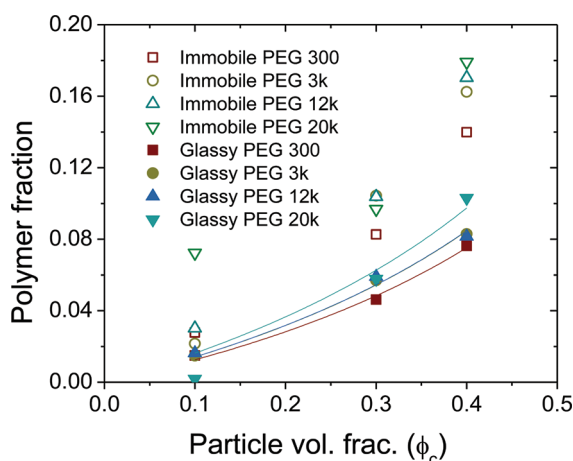


Figure 3. Glassy and total immobilized polymer fractions as a function of particle volume fraction with varying PEG molecular weight at 70°C and fitted curves.

curve can again be used to fix the shape parameters of the relaxation function used in the fits.

Multiple-Quantum NMR. For a complete account of the principles of MQ NMR as applied to polymers and other soft solids, the reader is again referred to the literature.²⁵ ^1H MQ NMR provides a measure of the time-dependent anisotropy of segmental dynamics, that can be described in terms of an orientation autocorrelation function of the second Legendre polynomial $C(t) = \langle P_2(\cos \theta(t))P_2(\cos \theta(0)) \rangle$, where θ is the instantaneous segmental orientation relative to the external magnetic field. The time-dependent correlation function measures the probability for a segment in a certain orientation at a reference time 0 to be in the same orientation at later time t . At short times, fast local fluctuations of polymer segments result in loss of conformational memory and thus $C(t)$ decays rapidly. At long times, however, rotational motions of polymer segments probing at the same time larger distances are hindered by the presence of topological constraints such as entanglements and cross-links. Therefore, the decay of $C(t)$ is much delayed, often forming a plateau (which extends to infinite time in network chains). The characteristic length scale of the topological constraints (such as the characteristic distance and chain length between two cross-links or anchoring points) is inversely related to the height of the plateau of $C(t)$, it is equal to the square of the local dynamic order parameter of the polymer backbone (S_b) which is typically on the order of a few percent. The nonisotropic nature of the chain motion means that the strong dipolar couplings among the ^1H mentioned above are not averaged to zero, but to a small yet finite value on the order of a few percent of the static-limit coupling D_{stat} . Specifically, S_b is proportional to the residual dipolar coupling, $D_{\text{res}} = S_b D_{\text{stat}}$, which is the central result of the MQ NMR experiment.

The major benefit of using MQ NMR as contrasted to more conventional experiments such as direct FID analysis or Hahn–echo relaxometry (which removes field-inhomogeneity effects from the FID) is that this technique can separate and remove relaxation effects due to the actual time scale of chain motion, meaning that the resulting D_{res} quantitatively reflects structural information, i.e., the inverse length of a network-like chain. In addition, the experiment even allows for the estimation of a possible distribution of D_{res} values, reflecting structural heterogeneity (variations in network chain lengths).

Note that the MQ experiment is closely related to the DQ filter sequence mentioned above; it also mainly measures the intensity of DQ coherences that are excitable due to the presence of dipolar couplings (even though in principle, higher quantum orders are involved at longer times, thus the name). The difference actually is the type of pulse sequence used, which is well-compensated and suitable for robust DQ excitation even when dipolar couplings are very small, and the excitation times are correspondingly long. Another difference is that the MQ experiment yields two signal functions as a function of the MQ pulse sequence time (τ_{DQ}), (i) the decaying sum MQ intensity (ΣMQ) and (ii) the double-quantum (DQ) build-up intensity. The ΣMQ decay is used for referencing of the signal; its decay reflects only the time scale of segmental orientation fluctuations, while the DQ build-up is governed by residual dipolar couplings (D_{res}) related to entanglements as well as cross-link effects arising from motions that are anisotropic on the ms time scale. The decay of the DQ signal at longer times depends again on the time scale of fast segmental modes, as well as on slower chain modes for the case of entangled chains. However, dividing DQ by ΣMQ yields a normalized DQ ($n\text{DQ}$) build-up function that in a sample containing a network depends exclusively on structural information as reflected in a well-defined D_{res} . In our experiments, τ_{DQ} was varied between 0.01 and 100 ms. Note that the pulse-sequence dependent minimum value of 0.1 ms is long enough to completely suppress any influence of the strongly coupled rigid regions, the signal of which decays within a few tens of μs due to higher-order effects. Therefore, the MQ experiments provide information only on the polymer component classified as mobile in our FID-based signal decompositions. The procedures for evaluating the corresponding results will be discussed in section III.

Hydroxyl Groups on the Silica Surface. A potential challenge in quantitatively interpreting the ^1H signals arises from the hydroxyl groups on the silica surface (silanol and other species) and the associated strongly bound water,^{44–46} which all contribute to the overall solid-like ^1H signals. This means that the actual glassy polymer fractions may be overestimated. The content of –OH groups in silica has been estimated by various methods.^{47–49} For example, Kim et al.⁴⁹ reported that the –OH group contents in silica were approximately 0.2–0.4 mmol/g. Converting into the mass fraction, ~0.03 wt % of silica corresponds to hydroxyls that can contribute to the rigid part signals or less in other references.⁴⁹

In the present study, for instance, PEG 300 at $\phi_c = 0.3$ has roughly 70% of PEG and 30% of silica. Since it has approximately 4% of glassy PEG (see Figure 3), the mass of glassy components in the total sample mass is determined to be 3 wt % ($=0.7 \times 4$ wt %). On the other hand, the OH mass fraction in silica is 0.01 wt % ($=0.3 \times 0.03$ wt %) which may contribute to the rigid glass-like polymer signals. Thus, we estimate that less than 1% of the rigid signal may come from proton spins associated with the particle, irrespective of the presence of PEG. This represents a safe margin, considering that water may be present in addition.

Small-Angle Neutron Scattering (SANS). SANS experiments were performed on the NG7 30 m SANS instrument at the NIST Center for Neutron Research, National Institute of Standards and Technology. Samples were loaded into 1 mm path length demountable titanium cells. The cell temperature was maintained to 70 ± 0.1 °C using the 10CB sample holder with a NESLAB circulating bath. A large range in scattering wave vector, q (0.001–0.1 Å⁻¹), was covered by combining the sector-averaged scattering intensity from two different instrument configurations at 4 and 13.5 m detector distance. SANS data reduction and analysis of the scattering intensity, I versus Q was performed using the SANS reduction and analysis program with IGOR Pro available from NIST. Detailed discussion of data reduction techniques is given in ref 50.

III. RESULTS AND DISCUSSION

A. FID Measurements. As discussed above, the FID signal immediately reflects the polymer mobility and thus reveals rigid and mobile signal contributions. Figure 2 shows typical results for PEG 20000 at $\phi_c = 0.4$ at 70 °C. Silica nanoparticles are stably dispersed in the PEG matrix in a miscibility window where neither depletion forces nor bridging lead to particle aggregation.^{38,51} Rheological experiments confirm that PEG adsorbs onto the silica particles both in the melt and in water-containing systems.^{51–53} Thus, differences in the FID curves among the different samples are associated with the presence of particles and the restrictions to polymer segmental motion due to physical adsorption of polymer segments to the particle surface. The quick initial decay reflects the proportion of glassy segments that hardly move and thus exhibit strong dipolar couplings. As described above, by using with the MAPE and DQ filters, we are able to accurately capture the relaxation function of the rigid and the mobile regions in the system. The MAPE-filtered signal provides a measure of the relaxation properties (shape of the decay function) of mobile chains in the bulk-like parts, and the DQ-filtered signal (detected using an MSE before detection) yields the relaxation properties of the glassy parts. In this process, we recognize contributions from spins that have intermediate relaxation times which arise due to an actual gradient in mobility as segments as we move away from the particle surface.^{16,54} We find an excellent representation of the data through a combination of stretched exponential functions of the form $\exp(-(t/\tau)^b)$ where τ is an apparent transverse relaxation time and b is a constant. At short times the decay is Gaussian for the segments that are in glassy environments ($b = 2$), while the more mobile phases require

$b < 2$. We find that three decay processes represent the data well and write the fitting function for the free induction decay as

$$I(t) = I_0(f_g \exp(-t/\tau_g)^{b_g} + f_i \exp(-t/\tau_i)^{b_i} + f_m \exp(-t/\tau_m)^{b_m}) \quad (1)$$

where I_0 is an amplitude factor, f_j is the fraction of the component j , and τ_j is the j th relaxation time with subscript g, i, and m denoting glassy, intermediate and mobile signal contributions, respectively. Fitting the DQ-filtered data reflecting the glassy part in Figure 2 with a single component yields $b_g = 2$ and $\tau_g = 0.034$ ms, while the long-time decay of the mobile parts as determined by the MAPE filter yields $b_m = 0.8$ and $\tau_m = 19.28$ ms. Fixing τ_g , b_g , τ_m , and b_m at the values determined from the DQ- and MAPE-filtered experiments, it is possible to fit the complete FID signal with eq 1. In this process, f_g , f_m , τ_i , and b_i remain free fit parameters, taking into account the constraint that $f_g + f_i + f_m = 1$.

In our fitting process, we first set $f_i = 0$ as shown in Figure 2b. This process fails to describe the data properly, implying the existence of an intermediate component with segmental relaxation time between the rigid/glassy limit and the mobile bulk-like phase. When we assume there is a third fraction with different mobility (different τ_g), we obtain good fits as shown in the same Figure 2b. Using three stretched exponential decays, it is possible to determine f_g and f_m . One notices that there are large uncertainties in the absolute values of τ_i and b_i as there is no independent *a-priori* information available for this intermediate fraction. Thus, there is typically more than one stable fit to the FID when τ_i and b_i are allowed to vary freely. With the obvious conditions that $\tau_g < \tau_i < \tau_m$ and $0.7 < b_i < 1.7$ for reasonable decay function reflecting intermediate relaxation processes, minima in residuals are found for (τ_i, b_i) to be (0.418 ms, 1.63) or (2.40 ms, 0.884). The choice of (τ_i, b_i) alters the fraction of spins that are found to relax with intermediate times, f_i .

However importantly, the glassy fraction is insensitive to the choice of (τ_i, b_i) . For example, $(\tau_i, b_i) = (0.418 \text{ ms}, 1.63)$ yields $f_g = 0.095$ and $f_i = 0.081$, while $(\tau_i, b_i) = (2.40 \text{ ms}, 0.884)$ yields $f_g = 0.097$ and $f_i = 0.51$ when other values are fixed to be same for the two cases. Consistently, we find that the fraction of intermediately relaxing polymers is associated with the choice of the matching point between intermediate and long-time relaxation processes such that different choices of (τ_i, b_i) result in variations in f_i and f_m but not f_g (additionally, it should be noted that the parameters τ_m and b_m change weakly with the used τ_{MAPE}). This means that the definitions of “intermediate” and “mobile” are to a degree *operational*, reflecting the simplification related to applying a 3-component model to a physical system that actually has a mobility gradient.

Particle Concentration and M_w Effects. Clear overall changes in the polymer relaxation properties are observed with growing particle volume fraction. In Figure 3, we show how both f_g and $f_g + f_i$ change with the filler volume fraction for different molecular weights. Here $f_g + f_i$ is referred as the total immobilized fraction (i.e., the fraction of spins that have relaxation properties different from those in the bulk). We note again that there are large yet systematic uncertainties in f_i . As a result, the total immobilized fraction can be interpreted phenomenologically by comparing different samples only when τ_i and b_i are held constant at different volume fractions.

For consistency, we have chosen $\tau_i = 0.418$ ms and $b_i = 1.63$ for all comparisons made.

For each PEG molecular weight, f_g increases with particle volume fraction. For PEG 300, $f_g \sim 0.02$ at $\phi_c = 0.1$, and it increases to $f_g = 0.079$ at $\phi_c = 0.4$. Similar trends are found in PEG 3000, 12000, and 20000 as shown in Figure 3. In the absence of particles where $f_g = 0$, glassy and intermediate fractions are, of course, absent. The near linearity of the data as a function of ϕ_c for each molecular weight in Figure 3 clearly indicates that the immobilized signal components are correlated with the presence of particles. Notably, at a fixed ϕ_c , f_g is virtually independent of molecular weight. If we assume adsorbed polymer chains are uniformly distributed on the silica particles, we can estimate a thickness of the glassy polymer layer by assuming the glassy response arises from an adsorbed polymer layer of a uniform density and thickness δ . The volume of this thin layer is written as $A_s\delta$ where $A_s = 6\phi_c/L$ is the specific surface area of silica in the composite, and L is the particle diameter. A_s has the unit of m^{-1} defined by surface area divided by the volume. Since the volume fraction of polymer is $1 - \phi_c$ and thus the fraction of glassy polymers in a total volume is $f_g \times (1 - \phi_c)$, one can find $f_g = 6\delta\phi_c/(L(1 - \phi_c))$. The fits to the data in Figure 3 yield nearly constant layer thicknesses of 0.8, 0.9, 0.9, and 1.0 nm for PEG 300, 3000, 12000, and 20000 respectively. Importantly, this excludes end-group effects, noting that PEG is terminated by $-OH$ groups, for which preferential adsorption cannot be excluded *a priori*. Obviously, lateral adsorption of chain segments dominates.

The statistical segment length of PEG is ~ 0.6 nm.^{55,56} The polymer radius of gyration varies from ~ 0.6 to 10 nm as the polymer molecular weight moves from 300 to 20000.^{55,56} These results clearly indicate that adsorbed polymer segments are completely immobilized on the dipolar-coupling time scale (kHz or slower); i.e., they are “glassy” in a layer of 1–2 polymer segments in width independent of polymer molecular weight. We expect that chains emanate from this adsorption layer, possibly forming either wide loops or bridges between particles,²⁴ the latter being elastically active, as proven below. The particles thus have the capability of behaving as multifunctional cross-links with M_w -independent polymer segment density on the particle surface.

The fraction of immobilized polymer segments at each ϕ_c shows variations depending on molecular weight. While the absolute value of $f_g + f_i$ is dependent on the choice of (τ_i, b_i) , if we hold the τ_i fixed as volume fraction and molecular weight are varied, we consistently find that $f_g + f_i$ grows with ϕ_c at fixed polymer molecular weight and, at fixed ϕ_c , with polymer molecular weight. Thus, higher- M_w polymers have a larger fraction of segments with proton spins that relax faster than in the bulk, indicating that as molecular weight increases, there is an increasing fraction of polymer segments whose mobility is lower than segments in the bulk. These results are expected in terms of the above-described picture, where parts of loop structures or chains linking different particles, and tails of the adsorbed polymer chains should have a mobility intermediate between glassy and bulk behavior. Adsorbing a polymer of greater molecular weight will restrict the mobility of a larger number of polymer segments. It could further be imagined that chain segments whose proton spins relax at given τ_i are embedded within mobile bulk-like chains. Because of the operational nature of the intermediate-component definition, and possible mobility gradients, we refrain from estimating the thickness of the layer showing intermediate relaxation times.

Nevertheless, we note that $f_g + f_i$ increases with volume fraction, with an apparent rapid increase in moving from $\phi_c = 0.3$ to $\phi_c = 0.4$ for the largest molecular weights.

We estimate the average spacing between the particles by embedding each particle of diameter L in a spherical volume of diameter B such that $\phi_c = (L/B)^3$. We then note that within this approximation, the average spacing between particle centers will be B and that B will go to L when the volume fraction reaches the maximum packing fraction (ϕ_m), which we further approximate as $\phi_m = 0.64$ —the random close packing value.⁵⁷ These approximations then lead to an average particle surface-to-surface spacing ($h = B - L$) normalized to the polymer radius of gyration (R_g) that can be written as $h/R_g = (L/R_g)((\phi_m/\phi_c)^{1/3} - 1)$. As h represents an average spacing, due to thermal motion, particle spacing is distributed around this value with particles experiencing much smaller and larger spacings. As the volume fraction increases, we expect h to approach R_g and segments trapped between particle surfaces to experience considerably greater restrictions to segmental motion than observed in the bulk. At $\phi_c = 0.4$, $h/R_g = 17$, 5.6, 2.8, and 2.1 for molecular weights of 300, 3000, 12,000 and 20,000 on average respectively when R_g is given by 2.0, 5.7, 9.9, and 12 nm, respectively. These estimates suggest the origin of the rapid increase in $f_g + f_i$ for polymers of molecular weights of 12000 and 20000 where ϕ_c increases from 0.3 to 0.4.

We summarize that introducing silica nanoparticles into PEG melts produces glassy layers of ~ 0.8 –1.0 nm thickness, and that this layer thickness is independent of volume fraction and polymer molecular weight. Furthermore, the volume fraction of polymer with restricted mobility increases with polymer molecular weight in a manner suggesting enhanced restrictions as particle surfaces reach separations characterizing the size of unperturbed polymer chains.

Effect of Temperature. In investigating the stability of particles in the presence of adsorbed polymer, temperature becomes an important variable for polymers suspended in a thermal solvent near phase-separation boundaries^{32,58} and in cases where variations in temperature alter the strength of polymer segment–particle surface attraction. Under these conditions, we expect polymer adsorption and polymer chain dynamics to be sensitive functions of temperature. On the other hand, in case of polymer melts as studied here, we are well away from phase boundaries, and we expect the polymer matrix to behave like a Θ solvent such that we would expect to see no change to the strength of adhesion with variations in temperature.³⁸

In the absence of solvent, we examined the polymer mobility at various molecular weights as we increased temperature between 70–100 °C. FID data was measured for all samples with $\phi_c = 0.4$ and fitted with three stretched exponential decays as explained above. Figure 4 shows glassy and total immobilized polymer fractions at 70 and 100 °C. For all polymer molecular weights, the glassy and total immobilized fractions are virtually independent of temperature. In other words, the fraction of polymer segments in the glassy state is unaltered by a temperature increase of 30 °C, suggesting that for the strongly adsorbed surface layers have a T_g higher than 100 °C.⁵⁴

It is noticeable that in the presence of solvent, the fraction of proton spins associated with glassy relaxation times decreases significantly as temperature increases (data not shown), which means that the water competes with the adsorbed PEO at the silica surface, possibly characterized by a temperature-dependent equilibrium and a certain adsorption–desorption kinetics.

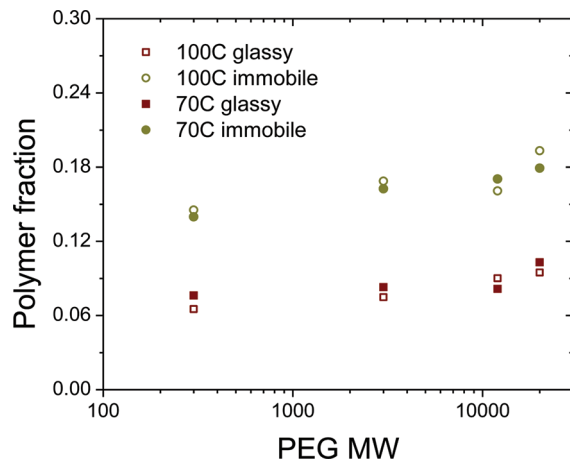


Figure 4. Polymer glassy and total immobilized fractions with varying molecular weight at two different temperature, 70 and 100 °C.

In contrast, in the melt system the mobility of the adsorbed glassy-layer polymer is insensitive to temperature, suggesting a long lifetime of the adsorption sites and an effectively athermal state of the silica particles in the PEG melt.

Effect of Dilution. Fixing particle volume fraction at 0.3, we investigated the effect of reducing the polymer concentration by diluting the polymer with D₂O. As shown in Figure 5, at 70

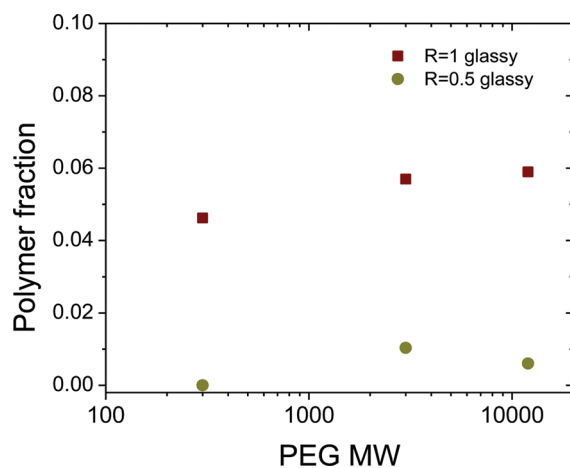


Figure 5. Glassy polymer fractions in polymer melt ($R_p = 1$) and polymer solution ($R_p = 0.5$) systems with varying molecular weight at 70 °C.

°C, f_g drops dramatically upon addition of water. This result directly demonstrates that the mobility of the polymer segments is greatly enhanced by the addition of solvent, and that much fewer segments are adsorbed to the particle surface.

Our previous studies revealed that at low temperature particle microstructure is weakly dependent on R_p for the same system studied here³² indicating that the state of particle dispersion and pair interactions are also weakly dependent on R_p . This lack of sensitivity of the microstructure to R_p was determined at 25 °C for PEG molecular weights of 400, and the results were found to be compatible with the strength of polymer segment-particle surface attraction and thus degree of polymer adsorption being independent of R_p . At room temperature, water is a good solvent and far below the lower critical solution temperature (LCST).⁵⁸ As a result, at room temperature the structural data are consistent with minimal

change in enthalpic gain of transferring monomer from the bulk to the surface in the presence or absence of water.

In the melt, the fraction of spins in the glassy state is independent of temperature. However, when the composite is diluted with water, our results show substantial changes in the fraction of protons with glassy relaxation times as temperature is varied from 30 to 70 °C. We attribute this to the system approaching the LCST, when water is no longer a good solvent for the PEG. For example, water-PEG 20000 mixtures show a lower critical solution temperature near 100 °C.⁵⁸ The approach of marginal solvent conditions as the temperature is raised has two consequences for the nanocomposite. First, as the LCST is approached, polymer-polymer attractions lead to increased polymer segment density fluctuations in the bulk. Second, the segments have a weaker tendency to adsorb to the particle surface. This acts to destabilize the particles by reducing the magnitude of the repulsive interparticle potential of mean force. This conclusion is supported by changes to particle microstructure indicating that polymer segments adsorb weakly to the particle surface.³²

B. MQ Experiments. We now turn to further characterizing the fraction that in the previous section has been classified as mobile, i.e., f_m in eq 1, and try to obtain a further distinction into chains subject to additional motional restrictions as arising from partial adsorption on the particle surfaces and topological constraints arising for the still mobile parts.

The main goal of the MQ experiments is to study polymer structures that contribute to elastically active networks such as cross-links or entanglements. We recall that the underlying principle of the measurements is that they essentially probe the long-time behavior of the time autocorrelation function $C(t)$ of the orientation of spin pairs in the mobile fraction, whereby chain segments with anisotropic mobility can be distinguished from isotropically mobile segments by their long-time plateau value in $C(t)$. As explained above, the MQ experiment generates two signal functions, ΣMQ and DQ. The DQ signal is proportional to $C(t)^{1/2}$ and corresponds to a direct measure of the residual dipolar coupling, D_{res} . At long times, it reaches an almost temperature-independent plateau value for network-like or well-entangled chains. The ΣMQ signal is mainly sensitive to the time scale of molecular motions that lead to long-time signal decay (relaxation), and can be used to correct the DQ signal for signal decay at long times, enabling the extraction of D_{res} . We expect D_{res} to increase with decreasing average length of the polymer chains spanning different particles (corresponding to an apparent network chain length).

Often it is not possible to isolate the signal due to active network-like or well-entangled material, as additional isotropically mobile components such as dangling chain ends or other defects also contribute to the ΣMQ signal function. A detailed discussion of these effects is given in ref 25. The effects of non-network material are particularly important when the polymer is only weakly cross-linked or entangled such that only a small fraction of actual network-like material exists.^{26,59} Under these conditions, the characterization of the elastically active material requires careful attention such that in data processing and analysis, corrections have to be applied. Details on these issues are given in ref 25 and the references cited therein. The analytical decay function of the ΣMQ signal can be written as

$$\Sigma MQ_{corr}(\tau_{DQ}) = \Sigma MQ(\tau_{DQ}) - f_B \exp^{-2\tau_{DQ}/T^{*2B}} - f_C \exp^{-2\tau_{DQ}/T^{*2C}} \quad (2)$$

where f_B and f_C are distinguishable defect fractions, and T_{2B}^* and T_{2C}^* are apparent relaxation times for the respective fractions, which are visible as slowly relaxing signal tails. We assign the shorter of the two relaxation times to T_{2B}^* , and thus associate f_B with components which experience more restrictions to the chain motion (e.g., by end fixation) that slow down the chain dynamics, while f_C represents the largest fraction in all samples, denoting the most mobile material which is mainly the unmodified bulk polymer.

Here we investigate polymers that are below the entanglement molecular weight or are weakly entangled such that at temperatures of interest, the terminal relaxation time is on the order of ms or less. Under these circumstances, in the absence of particles, none of the molecular weights of PEG studied showed indications of long-time residual dipolar couplings (i.e., that data were consistent with $DQ \sim 0$). However for samples with significant network-like components, we observe a significant dipolar-coupled ($DQ > 0$) fraction given by $f_{\text{net}} = 1 - f_B - f_C$.

Figure 6a shows an example of the effects of subtracting the different tail fractions from the ΣMQ signal. The corresponding exponential fits were performed on ΣMQ data in semi-logarithmic representations of the ΣMQ signal vs τ_{DQ} , in which

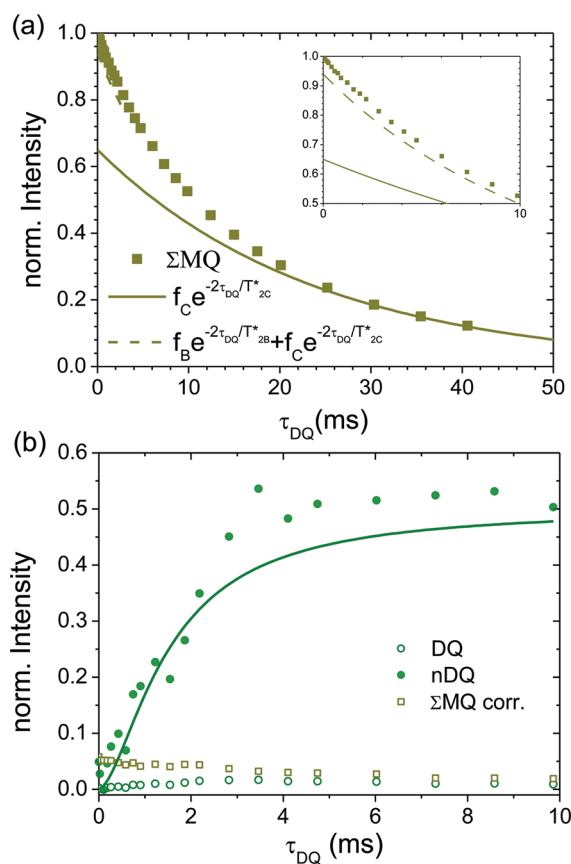


Figure 6. MQ NMR data decomposition for PEG 20000 $\phi_c = 0.4$ at 70 °C. (a) The full ΣMQ decay function and its fits to eq 2 for the determination of melt-like fractions (inset: expanded view for short times). (b) After subtraction of the defect fractions, the corrected data for ΣMQ reflects only the low network fraction ($f_{\text{net}} \approx 0.05$ as seen from the intercept). Empty squares and circles are for the ΣMQ and DQ signal functions, respectively, and filled circles denote the normalized DQ build-up curves ($n\text{DQ}$) characterizing the network-like component with its specific D_{res} . The solid curve is its fit to eq 3.

exponential tail components are easily identified as linear decays with very long relaxation times. Our PEG-silica nanocomposites are generally expected to have only a small fraction of network-like chains with short relaxation times due to the absence of actual cross-links and the relatively low polymer molecular weight, as noted above. This expectation is supported by the data in Table 1, where the ΣMQ signal decay shows large fractions of f_B and f_C and small network fractions. After subtraction, the ΣMQ signal only represents the network-like polymer segments, and a point-by-point division of the DQ signal by the ΣMQ signal is carried out to obtain the normalized DQ ($n\text{DQ}$) intensity build-up curve. The $n\text{DQ}$ intensity is analyzed and fitted with recently introduced build-up function,⁶⁰ taking into account a distribution coupling constants following ref 26:

$$n\text{DQ}(\tau_{\text{DQ}}) = p \int_0^\infty \frac{1}{2} \{1 - \exp(-(0.378D_{\text{res}}\tau_{\text{DQ}})^{1.5}\} \\ \cos[(0.583D_{\text{res}}\tau_{\text{DQ}})]P(D_{\text{res}}) \exp\left\{-\frac{\tau_{\text{DQ}}}{T_{2B}^*}\right\} \\ \text{d}D_{\text{res}} \quad (3)$$

We assume a gamma distribution function of residual couplings

$$P(D_{\text{res}}) = \frac{2}{\sqrt{\pi}} \sqrt{\frac{27|D_{\text{res}}|}{8\bar{D}_{\text{res}}^3}} \exp^{-3|D_{\text{res}}|/2(\bar{D}_{\text{res}})}$$

which accounts for the rather pronounced apparent inhomogeneities of the samples. The use of this distribution function is advantageous as its width is related to its average, which means that no additional fitting parameter is introduced. Its application to the given samples is justified by their similarity to the case of swollen networks which are characterized by substantial inhomogeneities, leading to D_{res} distributions of similar shape.⁶¹ Given the limited quality of our data, an exact quantification of the D_{res} distribution is not realistic. The results of the fitting (using $p = 1$ and $T_{2B}^* \rightarrow \infty$, *vide infra*) allows us to extract an average, apparent \bar{D}_{res} , and is shown in the Figure 6b as solid curve.

In some samples, in particular the lower- M_w PEG bulk samples, the $n\text{DQ}$ curves do not reach the theoretically expected plateau value of 0.5. In these samples, the data decays to zero at longer times (where the data quality is challenged by the division of low intensities). Such behavior is typical when the cross-link- or entanglement-induced anisotropy of motion is lost at longer (“intermediate”) times due to isotropic terminal relaxation (reptation, arm retraction, or rotations of larger branched structures, depending on the type of constraint to chain motion). In such cases, $C(t)$ has no clear plateau and reaches zero at long times. For the resulting $n\text{DQ}$ build-up function, this can be accounted for empirically by an additional exponential term decaying with T_{2B}^* , as done in ref 26.

However, a second possibility of too low values is that the tail subtraction was not complete in a sense that isotropically mobile fractions are not accounted for completely in the corrected ΣMQ signal. This can happen when isotropically moving chains (for instance again in large branched dangling structures) by coincidence exhibit a similar long-time ΣMQ decay as the network-like component. This is accounted for by the factor p in eq 3. One could then discuss a corrected network fraction $f_{\text{net}} \times p$. However, as our samples are very heterogeneous we are not in a position to distinguish effects of intermediate motions or nonseparated isotropic contributions.

Table 1. Results of Fits to Data from the Multiple-Quantum Experiments^a

MW	ϕ_c	R_p	T_{2C} (ms)	T_{2B} (ms)	f_C	f_B	f_{net}	p	$\bar{D}_{app}/2\pi$ (Hz)
20k	$\phi_c = 0.4$	$R_p = 1$	48.0	13.0	0.652	0.261	0.087	1.00	196
12k	$\phi_c = 0.4$	$R_p = 1$	42.0	13.0	0.824	0.118	0.059	1.00	180
3k	$\phi_c = 0.4$	$R_p = 1$	130	20.0	0.838	0.100	0.062	1.00	103
12k	$\phi_c = 0.3$	$R_p = 1$	58.0	27.0	0.674	0.302	0.023	0.753	82.0
3k	$\phi_c = 0.3$	$R_p = 1$	150	14.0	0.884	0.070	0.047	1.00	62.1
20k	$\phi_c = 0.1$	$R_p = 1$	73.3	12.9	0.857	0.116	0.027	0.901	84.4
12k	$\phi_c = 0.1$	$R_p = 1$	64.0	25.2	0.951	0.042	0.007	0.368	69.7
3k	$\phi_c = 0.1$	$R_p = 1$	213		0.956	—	—	—	—
20k	$\phi_c = 0$	$R_p = 1$	46.7		0.992	0.000	0.008	1.00	37.8
12k	$\phi_c = 0$	$R_p = 1$	65.2		0.982	0.000	0.018	0.457	32.7
12k	$\phi_c = 0.3$	$R_p = 0.5$	181		0.908	0.074	(0.018)	(0.443)	(49.1)
3k	$\phi_c = 0.3$	$R_p = 0.5$	159		0.906	—	(0.094)	(1.00)	(34.0)

^aNumbers in brackets are subject to a large uncertainty related to a low signal-to-noise ratio.

This is why we fit all data with eq 3 using $p \leq 1$ and $T_2^* \rightarrow \infty$ up to the maximum in nDQ. Noting that a series expansion of eq 3 for short times²⁵ yields $nDQ \propto p \bar{D}_{res}^2 \tau_{DQ}^2$, we simply absorb p into the apparent average $\bar{D}_{app} = \bar{D}_{res}(p)^{1/2}$, which we assign to the total network-like component.

Particle Concentration and MW Effect. Figure 7a, b and c show the nDQ build up curves and their fits to eq 3. Since residual dipolar couplings are the origin of the appearance of nDQ intensity build-up, we can interpret the \bar{D}_{app} values on the basis of their direct proportionality to the inverse elastic strand length between constraints.²⁵ Generally speaking, \bar{D}_{app} is a measure of the presence of factors hindering the isotropic chain motion, such as entanglements, and/or topological and physical cross-links. We notice that for the lower molecular weights at low particle loading in Figure 7b and 7c, the build-up curves do not reach the expected plateau, thus $p < 1$. For these cases, the \bar{D}_{app} represents an average that includes possibly isotropically mobile (but slowly moving and thus constrained) structures, yet remains comparable to the results on the samples exhibiting a clean network-like fraction, where $p = 1$.

For the PEG molecular weights studied, nDQ increases rapidly as particle volume fractions increase, as shown in Figures 7a-c, indicating a systematic increase in \bar{D}_{app} with volume fraction. For PEG3000 for $\phi_c < 0.1$, no detectable DQ data could be obtained (i.e., the ΣMQ signal was dominated by the isotropically mobile fractions B and C). This is expected because the entanglement molecular weight of PEG lies near 3000. Thus, the lack of a signal indicates a lack of entanglement effects even in the bulk. It is thus surprising that, as volume fraction is increased to 0.3–0.4 where the average surface-to-surface separation, h is less than $\sim 6R_g$, the residual dipolar coupling, \bar{D}_{app} , increases substantially. As shown in Table 1, for PEG3000, \bar{D}_{app} increases from 0 to 62.1 and 103 Hz as ϕ_c increases from 0.0 to 0.3 and 0.4, demonstrating a substantial increase of constraints to chain motion.

Thus, in bulk PEG 3000 we observe no evidence of entanglements (no residual dipolar coupling). However as the average surface-to-surface separation drops below $\sim 6R_g$, particles induce substantial residual orientational correlations, indicating the presence of network-like material. This may not necessarily be associated only with actual interparticle bridges, but also with loop structures with anchor points that are spatially separated (loops with adjacent anchoring points would not exhibit a finite \bar{D}_{app} as the whole loop could reorient almost isotropically). We also again emphasize that while the average separation may be $6R_g$, we expect a distribution of particle

separations with some particles experiencing much smaller separations, allowing for actual bridging chains.

When polymer is substantially above the entanglement molecular weight M_e , such as in PEG 12000 and 20000, the nDQ build-up curves rise even in the absence of particles due to the presence of entanglement constraints in bulk polymer. However, this is a weak effect (pertaining to a very small apparent chain-center fraction, see the f_C values in Table 1). Adding particles leads to a noticeable formation of network-like components, as indicated by quickly rising nDQ signals and correspondingly increased \bar{D}_{app} . We now analyze the molecular weight-dependent effect in detail by comparing with changes in composite rheology.

We first note that increasing the molecular weight affects not only the apparent network fraction but also the magnitude of the dipolar coupling. For all M_w , f_{net} , and \bar{D}_{app} follow the same trend, indicating that with increasing particle concentration, both the apparent network fraction and the apparent cross-link density (inverse the strand length) increase. As demonstrated above with the FID for melt systems, the polymer is adsorbed to the particle surface, forming a glassy layer with a thickness weakly dependent on molecular weight. The result will be a corona of loops and dangling polymers associated with this adsorbed layer, the thickness of which is expected to increase with molecular weight. Supporting this hypothesis, Anderson et al.^{51,52} showed that at low volume fraction the viscosity of suspensions of silica particles in PEG melts followed the behavior expected for suspension of hard spheres as if silica particles had a diameter of $L(1 + 2.8R_g/L)$. In their studies, R_g was varied over 1 order of magnitude.⁵¹ As the volume fraction was increased, Anderson defined a series of volume fractions where rheological transitions take place. These transitions occurred at approximately constant values of h/R_g and were associated with primary or secondary “entanglements” that bridge the interparticle gap. Of significance here is the critical volume fraction Anderson associated with entanglements, ϕ_{ce} which occurred when $h \sim 6R_g$. Substantial changes were also observed when the strongly adsorbed polymer layers overlapped at ϕ^* where $h \sim 3.6R_g$. While Anderson associated the rheological transitions with entanglements, the increased \bar{D}_{app} observed by us at lower particle volume fractions (large particle spacings) may not so much be related to actual network-like bridging chains, but to those loop structures with remote anchoring points. Again, we note that loops of chains with closely neighboring anchoring points, as long as they are not

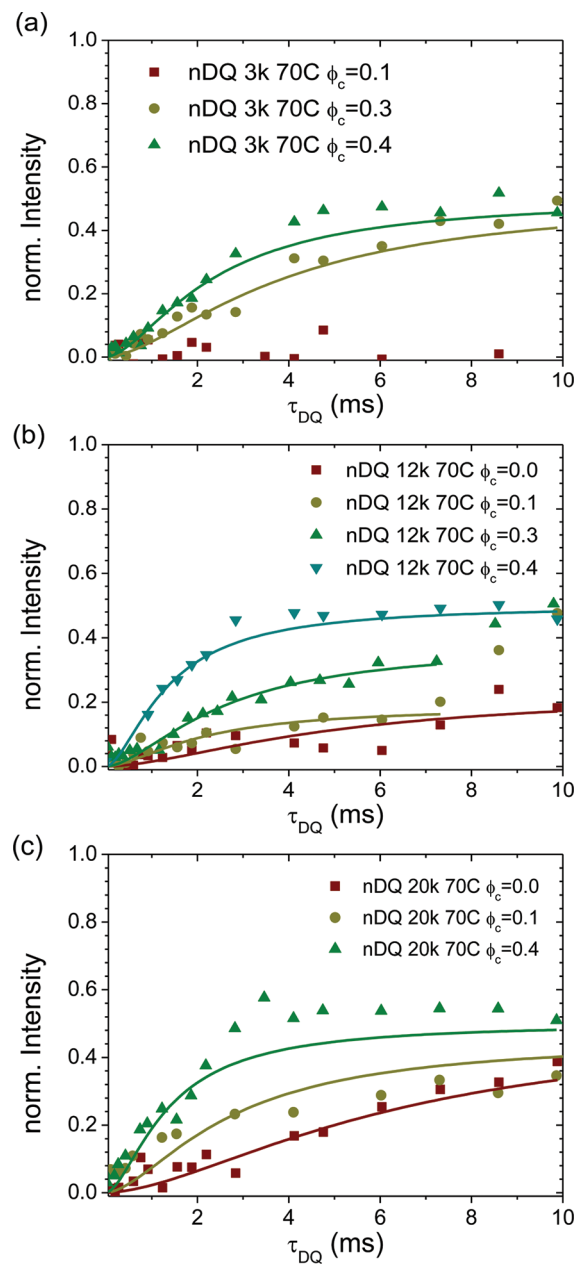


Figure 7. nDQ build-up curves of Silica-PEG composites with varying particle volume fractions at 70 °C: (a) PEG 3000, (b) PEG 12000, and (c) PEG 20000.

trapped by other chains, are able to perform near-isotropic fluctuations.

In addition, Anderson et al. observed that a rheological transition occurs when the effective volume fraction defined as $(\phi_c(1 + 2.8R_g/L)^3)$ equals 0.58, at which the suspension of effective hard spheres will form a glass (ϕ_g). This glassy transition is observed most easily when $\phi_g < \phi_{c,e} < \phi^*$. For molecular weights less than 1000 in PEG and $L = 44$ nm, this condition was met and colloidal glass transitions were observed as the effective volume fraction exceeded a value of 0.58.⁶² On the other hand, for larger molecular weights $\phi_{c,e} < \phi_g$, the colloidal glass transition was obscured and changes to composite flow properties were attributed to changes to polymer dynamics induced by the presence of closely spaced particles. For PEG20000, $\phi_{c,e} = 0.012$, $\phi^* = 0.192$, and $\phi_g = 0.22$, while we estimate that for PEG12000, $\phi_{c,e} = 0.04$, $\phi^* \sim$

0.25, and $\phi_g = 0.23$ and for PEG3000, $\phi_{c,e} = 0.17$, $\phi^* \sim 0.38$ and $\phi_g \sim 0.38$.⁵¹

Anderson's assignment of changes in rheological behavior to the ability of polymers to entangle had no molecular support. The multiple-quantum experiments carried out here now provide evidence that particles induce constraints to the polymer chain relaxation as the volume fraction is raised.

For PEG 3000, $\phi_c = 0.1$ is below $\phi_{c,e} = 0.17$. Anderson observed that under these conditions suspensions had the flow properties of a hard-sphere suspension with diameters slightly larger than the bare particle (i.e., particles had diameters of $L(1 + 2.8R_g/L)$). Anderson thus predicts no changes to bulk relaxation properties and as shown in Figure 8a, we see no

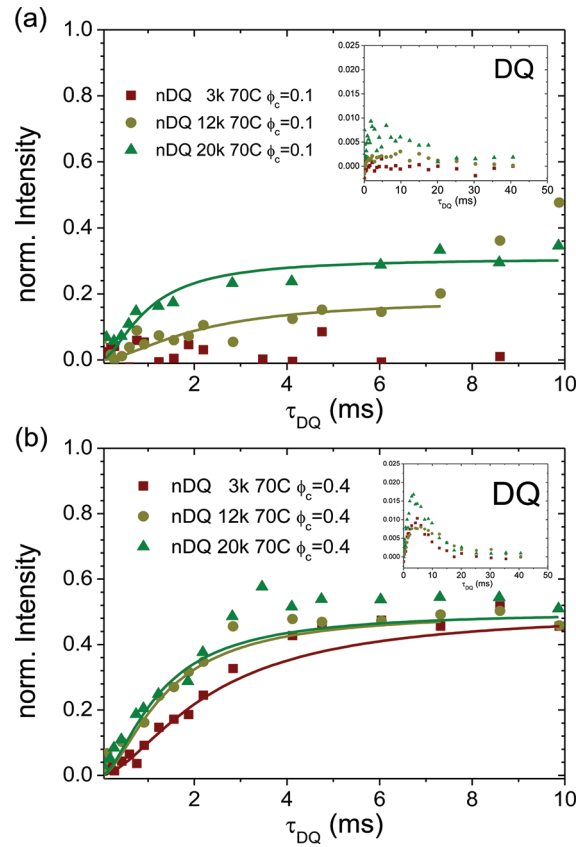


Figure 8. nDQ build-up curves and unnormalized DQ intensity (insets) of Silica-PEG composites with varying polymer molecular weight at 70 °C: (a) $\phi_c = 0.1$; (b) $\phi_c = 0.4$.

surface-induced changes to f_{net} or \bar{D}_{app} . On the other hand, for both PEG 12000 and 20000, $\phi_c = 0.1$ is substantially above $\phi_{c,e}$ (=0.04 and 0.012, respectively) where Anderson assigned changes to composite elastic effects to particle-induced polymer "entanglements". In support of this conclusion, we observe residual dipolar coupling suggesting that polymer dynamics are being substantially altered due to the formation of a network-like signal, most probably loops with separated ends or topologically trapped loops (Figure 8a). This interpretation suggests substantial changes in composite elasticity can be associated with loop structures. We are left concluding that even when the particles are spaced by a large distance compared to R_g particle surfaces significantly alter the polymer dynamics, mimicking network formation and that these alterations are associated with alterations in composite viscoelasticity.

Anderson assigned his observations of changes to viscoelastic response to entanglements that are active in the interparticle gaps. We cannot confirm this suggestion or differentiate it from a mechanism where the presence of large amount of closely spaced surfaces induces the polymer to form actual bridges. Nevertheless, our residual dipole coupling results demonstrate that near the volume fractions where Anderson reports changes in mechanical behavior, significant fractions of network-like chains appear. Therefore, we conclude that in the PEG-silica composites particles can induce network formation when particle are spaced at distances that scale with the polymer radius of gyration. We note that for PEG3000, entanglement effects are not observed in the pure polymer, but at $\phi_c = 0.3$, there is a rapid buildup of the nDQ curve that levels out at the expected 0.5 plateau, indicating the presence of a well-defined network-like fraction with significant residual dipolar coupling (Figures 7a and 8b). This occurs where interparticle spacing approaches that characterizing the colloidal glass transition of effective hard spheres of diameter L ($1 + 2.8R_g/L$) (i.e., at a volume fraction where bound polymer layers will strongly interact), demonstrating the dramatic ability of a strongly adsorbing surface to alter polymer network formation.

At $\phi_c = 0.4$ where ϕ_c is above ϕ^* and ϕ_g for all PEG molecular weights, all three composites show the presence of a well-defined network-like fraction, as indicated in Figure 8b. Because of the reduced surface-to-surface separations with increasing ϕ_c , the effective cross-link density increases, leading to larger \bar{D}_{app} and faster nDQ build-up as compared to the cases with lower ϕ_c . The difference of \bar{D}_{app} from the highest two molecular weights is much smaller than that from the lowest M_w . However, the increased degree of polymerization of the 20k sample leads to a larger fraction of polymer being trapped in the network. From these studies we conclude that polymer networks become denser with increasing particle volume fraction and with increasing the PEG molecular weight.

Dilution Effect. Diluting polymer nanocomposites with solvent clearly reduces the fraction of segments trapped in a glassy state as shown above. In agreement with this indication of a weaker influence of the surface on polymer dynamics as R_p is reduced from 1 to 0.5, we find that at $\phi_c = 0.3$ and $R_p = 0.5$ with PEG3000 and PEG12000 both nDQ build-up curves become much noisier due to the very low values of f_{net} as shown in Figure 9. Even though the fits to the nDQ build-up curves at $R_p = 0.5$ were somewhat challenged due to the low signal-to-noise ratio, leading to larger potential uncertainties in the fit results, it is clear from fit results and the build-up curves themselves that the behavior is not qualitatively different from the case of $R_p = 1$. The noticeable decrease of \bar{D}_{app} can be attributed to the dilution of polymer by solvent, involving a decrease in the number and/or the length of loop and bridge chains. We note that by heating to 70 °C the FID experiments indicate a dramatic reduction in the fraction of proton spins trapped in a glassy state at the particle surface suggesting a correlation between strength of segment formation and surface enhanced network formation.

C. Connections to the Particle Dispersions and Physical Properties. From the FID and MQ-NMR experiments, one understands that there are substantial changes in polymer mobility and network formation as R_p is reduced from 1 to 0.5. The origin of the varying polymer mobility and network formation observed in the NMR experiments results from changes in the way polymer is bound to the particle

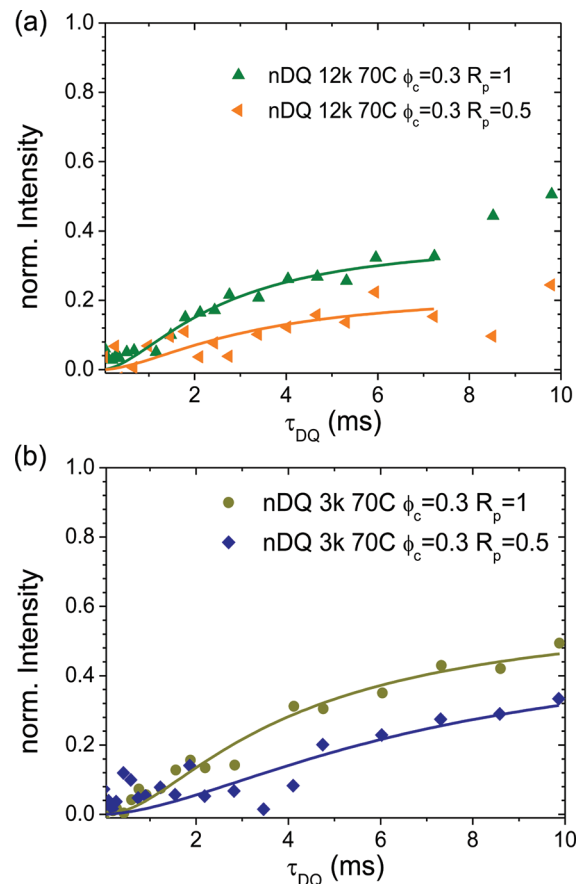


Figure 9. nDQ build-up curves of Silica-PEG composites in bulk ($R_p = 1$) and with solvent ($R_p = 0.5$) at a fixed $\phi_c = 0.3$ at 70 °C: (a) PEG 12000; (b) PEG 3000.

surface. We anticipate that these changes should be reflected in particle microstructure.

In Figure 10 we show the inverse osmotic compressibility ($1/S(0)$) as a function of particle volume fraction for PEG 8000 at $R_p = 1$ and $R_p = 0.5$ obtained from SANS experiments. The detailed experimental method to extract the inverse osmotic

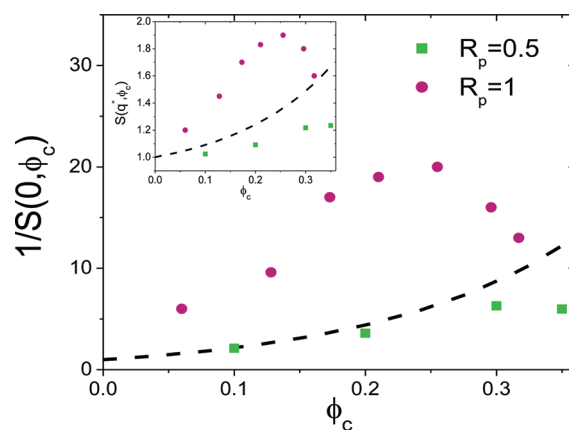


Figure 10. Experimental inverse osmotic compressibilities ($1/S(0,\phi_c)$) as a function of particle volume fraction (ϕ_c) for different $R_p = 0.5$ and 1 for PEG 8000, at 70 and 75 °C, respectively. Inset: height of the cage peak of the particle structure factor ($S(q^*,\phi_c)$) as a function of ϕ_c under the same conditions. The data for $R_p = 1$ is taken from ref 51. The dashed line is the curve expected for hard spheres.

compressibility from scattering experiments can be found in refs 31 and 41. The initial observation is that particles are stable with no indication of aggregation. These results are interpreted as indicating that the strength of polymer segment/particle surface interactions are sufficient to produce strong thermodynamically stable adsorbed polymer layers.^{31,32} The insert of Figure 10 shows the height of the first peak in $S(q^*)$ as a function of volume fraction. The height of this peak is a measure of the coherence of the first nearest-neighbor shell. As the coherence increases, the first nearest-neighbor shell becomes better defined and particle order increases. Greater coherence is associated with more strongly interacting particles. These measurements were made at 75 and 70 °C, respectively for $R_p = 1$ and $R_p = 0.5$, and the dramatic changes seen between $R_p = 1$ and $R_p = 0.5$ indicate that the solvent is playing a substantial role in altering suspension microstructure.

An increase in $1/S(0)$ indicates that the particle subsystem becomes less compressible, while an increasing $S(q^*)$ suggest that the particle arrangement is more structured: both observations are consistent with an increasingly repulsive potential of mean force. Two distinct features are found in Figure 10. First, when particles are suspended in the PEG 8000 melt, $1/S(0)$ is a nonmonotonic function of particle volume fraction. Without any signs of aggregation, at low ϕ_c the system becomes less compressible with increasing ϕ_c . However, near $\phi_c = 0.25$ $1/S(0)$ passes through a maximum. We note that this transition occurs at volume fractions where previous studies suggest polymer bound to the particle surfaces begin to interact and we correspondingly see substantial increases in residual dipolar coupling (nDQ intensity). Thus, while polymer network formation does not destabilize the particles, changes in particle microstructure can be interpreted as suggesting that particles experience a different environment consistent with a reduction in strength of repulsion in the potentials of mean force. The same trends are observed in $S(q^*)$ from the inset of Figure 10.

Second, as R_p decreases from 1 to 0.5, both $1/S(0)$ and $S(q^*)$ are greatly reduced. These features indicate particles experience weaker repulsive potentials of mean force upon dilution at 70 °C. These observations are consistent with weaker adsorption of polymer segments to the particle surfaces³⁸ and the decreased amount of glassy adsorbed PEG observed in the FID experiments.

Overall, through the comparisons to the structure factor from scattering, one can clearly see that the polymer network formation is directly correlated with the state of particle dispersion thus connecting network formation with particle stability and phase separation. The impact of particle-mediated changes in polymer dynamics, leading to substantial changes of the rheological behavior, is clearly evident in Figure 1. At $\phi_c = 0.314 > \phi^*$ polymer nanocomposite melts of PEG 8000 behave like brittle gels (Figure 1a). However, at $R_p = 0.5$ at the same volume fraction the composite retains liquid-like properties (Figure 1b). While the polymer is diluted, it remains in the concentrated region such that chains will remain entangled. However, the weak coupling of the polymer segments with the particle surfaces allows for enhanced polymer relaxations and thus the composite remains in a liquid-like state.

IV. SUMMARY

The goal of this current study was to observe changes in polymer dynamics in nanocomposites composed of silica and PEG with varying particle volume fraction, polymer molecular

weight, temperature and dilution with a low molecular weight solvent. We show that for all molecular weights studied, physical adsorption of PEG segments to the silica surface produces a glassy polymer layer. The fraction of polymer segments in a glassy state is invariant with polymer molecular weight, implying the layer thickness of glassy segments is independent of polymer molecular weight. Furthermore, in the polymer melt the fraction of segments in the glassy layers does not change as the temperature is increased from 70 to 100 °C, suggesting that the adsorption is sufficiently strong and that the glass transition temperature for this layer is greater than 100 °C. If the nanocomposites are diluted with solvent at high temperature, we observe significant changes polymer dynamics indicating substantially fewer segments that are in a glassy state and adsorbed on the particle surface.

MQ-NMR experiments enabled us to examine the development of highly entangled and network-like components with increasing molecular weight and filler concentration, and again a decay upon solvent dilution. At and above the entanglement molecular weight, the residual dipolar coupling grows with volume fraction. Near the entanglement molecular weight, there is no evidence of entanglements at low particle volume fractions. However, as the volume fraction grows, such that the average particle spacing approaches distances at which bound polymer players can interact, there is a strong increase in the network-like polymer formation. The fraction of polymer segments in the particle-induced network grows with polymer molecular weight and filler concentration. The onset of polymer network formation correlates with changes in composite rheology (onset of a rapid increase in elasticity with volume fraction and the onset of multiple yielding events). When the polymer is diluted with solvent, the glassy layer thickness and the apparent network-like polymer fraction are greatly reduced, showing that at the temperatures studied, the solvent competes with polymer segments for the particle surface. Because the polymer is more weakly associated with the particle surface, network formation is suppressed, indicating that only for sufficiently strong polymer segment-particle surface interaction strength will the presence of particles result in mechanical reinforcement beyond simple hydrodynamic predictions.

■ AUTHOR INFORMATION

Corresponding Author

*E-mail: (K.S.) kay.saalwaechter@physik.uni-halle.de; (C.F.Z.) czukoski@illinois.edu.

Present Address

[§]Department of Chemical and Biological Engineering, Princeton University, Princeton, NJ 08544

Notes

The authors declare no competing financial interest.

■ ACKNOWLEDGMENTS

This work was supported by the Nanoscale Science and Engineering Initiative under NSF Award DMR-0642573. We acknowledge the support of the National Institute of Standards and Technology, U.S. Department of Commerce, in providing the neutron research facilities used in this work. H.W.M. and K.S. thank the Deutsche Forschungsgemeinschaft (SA 982/6-1) for financial support.

■ REFERENCES

- (1) Ajayan, P. M.; Schadler, L. S.; Braun, P. V. *Nanocomposite Science and Technology*; Wiley-VCH: Weinheim, Germany, 2003.
- (2) Ebbesen, T. W.; Lezec, H. J.; Hiura, H.; Bennett, J. W.; Ghaemi, H. F.; Thio, T. *Nature* **1996**, *382*, 54.
- (3) Oberdisse, J. *Soft Matter* **2006**, *2*, 29.
- (4) Zhang, W.; Dehghani-Sanij, A. A.; Blackburn, R. S. *J. Mater. Sci.* **2007**, *42*, 3408.
- (5) Akcora, P.; Kumar, S. K.; Moll, J.; Lewis, S.; Schadler, L. S.; Li, Y.; Benicewicz, B. C.; Sandy, A.; Narayanan, S.; Ilavsky, J.; Thiagarajan, P.; Colby, R. H.; Douglas, J. F. *Macromolecules* **2009**, *43*, 1003.
- (6) Aranguren, M. I.; Mora, E.; Degroot, J. V.; Macosko, C. W. *J. Rheol.* **1992**, *36*, 1165.
- (7) Sen, S.; Thomlin, J. D.; Kumar, S. K.; Keblinski, P. *Macromolecules* **2007**, *40*, 4059.
- (8) Bansal, A.; Yang, H.; Li, C.; Benicewicz, B. C.; Kumar, S. K.; Schadler, L. S. *J. Polym. Sci. Polymer Phys.* **2006**, *44*, 2944.
- (9) Mark, J. E.; Erman, B.; Eirich, F. R. *The Science and Technology of Rubber*; Elsevier: Amsterdam, 2005.
- (10) Wang, M.; Hill, R. J. *Soft Matter* **2009**, *5*, 3940.
- (11) Montes, H.; Lequeux, F.; Berriot, J. *Macromolecules* **2003**, *36*, 8107.
- (12) Berriot, J.; Montes, H.; Lequeux, F.; Long, D.; Sotta, P. *Macromolecules* **2002**, *35*, 9756.
- (13) Cohen-Addad, J. P.; Roby, C.; Sauviat, M. *Polymer* **1985**, *26*, 1231.
- (14) Kirst, K. U.; Kremer, F.; Litvinov, V. M. *Macromolecules* **1993**, *26*, 975.
- (15) Litvinov, V. M.; Zhdanov, A. A. *Vysokomol. Soedin. A* **1987**, *29*, 1021.
- (16) Papon, A.; Saalwächter, K.; Schäler, K.; Guy, L.; Lequeux, F.; Montes, H. *Macromolecules* **2011**, *44*, 913.
- (17) Sun, Y.; Zhang, Z.; Moon, K.-S.; Wong, C. P. J. *Polym. Sci., Polym. Phys.* **2004**, *42*, 3849.
- (18) Ash, B. J.; Schadler, L. S.; Siegel, R. W. *Mater. Lett.* **2002**, *55*, 83.
- (19) Robertson, C. G.; Lin, C. J.; Rackaitis, M.; Roland, C. M. *Macromolecules* **2008**, *41*, 2727.
- (20) Krutyeva, M.; Martin, J.; Arbe, A.; Colmenero, J.; Mijangos, C.; Schneider, G. J.; Unruh, T.; Su, Y.; Richter, D. *J. Chem. Phys.* **2009**, *131*, 174901.
- (21) Martín, J.; Krutyeva, M.; Monkenbusch, M.; Arbe, A.; Allgaier, J.; Radulescu, A.; Falus, P.; Maiz, J.; Mijangos, C.; Colmenero, J.; Richter, D. *Phys. Rev. Lett.* **2010**, *104*, 197801.
- (22) Cohen-Addad, J. P.; Viallat, A. *Polymer* **1986**, *27*, 1855.
- (23) Cosgrove, T.; Turner, M. J.; Thomas, D. R. *Polymer* **1997**, *38*, 3885.
- (24) Litvinov, V. M.; Barthel, H.; Weis, J. *Macromolecules* **2002**, *35*, 4356.
- (25) Saalwächter, K. *Prog. Nucl. Mag. Res. Spectrosc.* **2007**, *51*, 1.
- (26) Ţerbescu, A.; Saalwächter, K. *Polymer* **2009**, *50*, 5434.
- (27) Gee, R. H.; Maxwell, R. S.; Balazs, B. *Polymer* **2004**, *45*, 3885.
- (28) Maxwell, R. S.; Balazs, B.; Cohenour, R.; Prevedel, E. *Macromol. Symp.* **2003**, *202*, 291.
- (29) Barthel, H. *Colloid. Surf. A* **1995**, *101*, 217.
- (30) Viallat, A.; Cohen-Addad, J. P.; Pouchelon, A. *Polymer* **1986**, *27*, 843.
- (31) Kim, S. Y.; Hall, L. M.; Schweizer, K. S.; Zukoski, C. F. *Macromolecules* **2010**, *43*, 10123.
- (32) Kim, S. Y.; Zukoski, C. F. *Langmuir* **2011**, *27*, 10455.
- (33) Kim, S. Y.; Zukoski, C. F. *Soft Matter* **2012**, *8*, 1801.
- (34) Kim, S. Y.; Schweizer, K. S.; Zukoski, C. F. *Phys. Rev. Lett.* **2011**, *107*, 225504.
- (35) Klonos, P.; Pissis, P.; Gun'ko, V. M.; Kyritsis, A.; Guzenko, N. V.; Pakhlov, E. M.; Zarko, V. I.; Janusz, W.; Skubiszewska-Zięba, J.; Leboda, R. *Colloid. Surf. A* **2010**, *360*, 220.
- (36) Napolitano, S.; Wübbenhorst, M. *Nat. Commun.* **2011**, *2*, 260.
- (37) Serghei, A.; Kremer, F. *Macromol. Chem. Phys.* **2008**, *209*, 810.
- (38) Hall, L. M.; Anderson, B. J.; Zukoski, C. F.; Schweizer, K. S. *Macromolecules* **2009**, *42*, 8435.
- (39) Mauri, M.; Thomann, Y.; Schneider, H.; Saalwächter, K. *Solid State Nucl. Magn. Reson.* **2008**, *34*, 125.
- (40) Stober, W.; Fink, A.; Bohn, E. *J. Colloid Interface Sci.* **1968**, *26*, 62.
- (41) Kim, S. Y.; Zukoski, C. F. *Langmuir* **2011**, *27*, 5211.
- (42) Israelachvili, J. N. *Intermolecular and Surface Forces*; Academic: London, 1995.
- (43) Demco, D. E.; Johansson, A.; Tegenfeldt, J. *Solid State Nucl. Magn. Reson.* **1995**, *4*, 13.
- (44) Saalwächter, K.; Krause, M.; Gronski, W. *Chem. Mater.* **2004**, *16*, 4071.
- (45) Kinney, D. R.; Chuang, I. S.; Maciel, G. E. *J. Am. Chem. Soc.* **1993**, *115*, 6786.
- (46) Bronnimann, C. E.; Zeigler, R. C.; Maciel, G. E. *J. Am. Chem. Soc.* **1988**, *110*, 2023.
- (47) Ek, S.; Root, A.; Peussa, M.; Niinistö, L. *Thermochim. Acta* **2001**, *379*, 201.
- (48) Holík, M.; Matějková, B. *J. Chromatogr. A* **1981**, *213*, 33.
- (49) Kim, J. M.; Chang, S. M.; Kong, S. M.; Kim, K. S.; Kim, J.; Kim, W. S. *Ceram. Int.* **2009**, *35*, 1015.
- (50) Kline, S. R. *J. Appl. Crystallogr.* **2006**, *39*, 895.
- (51) Anderson, B. J.; Zukoski, C. F. *Macromolecules* **2009**, *42*, 8370.
- (52) Anderson, B. J.; Zukoski, C. F. *Macromolecules* **2008**, *41*, 9326.
- (53) Liu, S. F.; Legrand, V.; Gourmand, M.; Lafuma, F.; Audebert, R. *Colloids Surf. A* **1996**, *111*, 139.
- (54) Papon, A.; Montes, H.; Hanafi, M.; Lequeux, F.; Guy, L.; Saalwächter, K. *Phys. Rev. Lett.* **2012**, *108*, 065702.
- (55) Flory, P. J. *Principles of Polymer Chemistry*; Cornell University: Ithaca, NY, 1953.
- (56) Grosberg, A. Y.; Khokhlov, A. R. *Statistical Physics of Macromolecules*; AIP Press: Melville, NY, 1994.
- (57) Bernal, J. D.; Mason, J. *Nature* **1960**, *188*, 910.
- (58) Saeki, S.; Kuwahara, N.; Nakata, M.; Kaneko, M. *Polymer* **1976**, *17*, 685.
- (59) Saalwächter, K.; Gottlieb, M.; Liu, R.; Oppermann, W. *Macromolecules* **2007**, *40*, 1555.
- (60) Chasse, W.; Lopez Valentin, J.; Genesky, G. D.; Cohen, C.; Saalwächter, K. *J. Chem. Phys.* **2011**, *134*, 044907.
- (61) Saalwächter, K.; Sommer, J. U. *Macromol. Rapid Commun.* **2007**, *28*, 1455.
- (62) Anderson, B. J.; Zukoski, C. F. *J. Phys.-Condes. Matter* **2009**, *21*, 164216.